PROCEEDINGS, 49th Workshop on Geothermal Reservoir Engineering
Stanford University, Stanford, California, February 12-14, 2024
SGP-TR-227

The combined effect of mineral dissolution/precipitation and matrix thermal contraction on fracture aperture in enhanced geothermal systems: a reactive transport approach

Hannah S. Gatz-Miller, Jennifer M. Frederick and Thomas S. Lowry

1515 Eubank Ave. SE, Albuquerque, NM 87185

hsgatzm@sandia.gov

Keywords: Enhanced Geothermal Systems (EGS), THCM modeling, reactive transport, fracture flow, numerical modeling

ABSTRACT

Thermal contraction, mineral dissolution, and secondary mineral precipitation can all affect fracture aperture in enhanced geothermal systems (EGS). For this work, the reactive transport code PFLOTRAN was used to examine the combined effect of both mineral dissolution/precipitation and mechanical thermal contraction of the rock matrix on effective permeability of a fracture zone. PFLOTRAN, which can already consider mineral kinetics and other geochemical processes, was further developed to include the effects of thermal contraction of a rock matrix and the resulting change in fracture aperture, in an equivalent continuous porous medium (ECPM) representation. A single horizontal fracture was represented in PFLOTRAN as a zone of distinct high porosity and permeability in a domain otherwise dominated by low permeability crystalline rock and, from these initial conditions, four 2D simulations (thermal-hydrological, thermal-hydrological-mechanical, thermal-hydrological-chemical, and thermal-hydrological-chemical-mechanical), were run in PFLOTRAN to observe changes in fracture aperture and effective permeability over time. It was found that while mineral precipitation decreased effective permeability of the fracture zone by half an order of magnitude, thermal contraction increased effective permeability by nearly two orders of magnitude, overriding the effects of mineral precipitation, with implications for pumping and thermal drawdown in enhanced geothermal systems. These results will be considered as part of the larger techno-economic model GT-Mod, to speak to the long-term power generating potential and economic practicality of EGS as a carbon neutral energy source.

1. INTRODUCTION

Enhanced Geothermal Systems (EGS) represent a significant potential for geothermal energy usage worldwide (Olasolo et al. 2016). Hot dry rock is fractured deep in the subsurface and water or other fluid (e.g. CO_2) is injected, removing heat from the surrounding rock as it moves preferentially through the fractures before returning to the surface for use in power generation (Gringarten et al. 1975; Olasolo et al. 2016; Feng et al. 2021). Over time, thermal drawdown results in limited returns in heat to the surface and thus power production (Gringarten et al. 1975). As changes in fluid outflow rate and temperature significantly affect the quantity of power produced, understanding changes in fracture aperture geometry through which the fluid migrates, is crucial in determining the longer-term economic viability of EGS (Lima et al. 2019; Huang et al. 2020; Dobson et al. 2021; Chen et al. 2023).

Fracture geometry and aperture width can be affected by both physical and chemical processes (Deng and Spycher 2019; Yin et al. 2019) leading to changes in preferential flow as well as flow velocity and, ultimately with respect to EGS, heat transfer. As matrix material cools and contracts, fracture aperture may increase (Deng and Spycher 2019; Deng et al. 2022). Concurrently, dissolution of matrix minerals and reprecipitation of secondary minerals on the facture face can cause further variation in porosity and permeability of the fracture zone, both decreasing and increasing permeability in different locations. The rate and location along the fracture of dissolution and re-precipitation is dependent on several factors including matrix mineralogy, the geochemistry of the injection fluid, the thermal environment, and the flow velocity (Singurindy and Berkowitz 2005; Li et al. 2008; Rawal and Gassemi 2008; Steefel and Hu 2022).

Previous work has explored the effect of thermal expansion and contraction on fractured rock using coupled Thermal-Hydraulic-Mechanical finite element models (Salimzadeh et al. 2018). The effect of mineral precipitation and dissolution on fractured rock has also been explored using both reactive transport and other numerical simulations (Xu et al. 2003; Li et al. 2008; Rawal and Gassemi 2008; Ogata et al. 2018; Steefel and Hu 2022). However, the combination of the mechanical and geochemical processes and their effect on the fluid flow path and thermal drawdown has not yet been investigated together in a reactive transport context. In this work, we use the reactive transport code PFLOTRAN to simulate fluid flow through a single fracture at 4000 meters (m) depth, including both mineral dissolution/precipitation and matrix thermal contraction in the simulations to investigate the combined effect of both processes on fracture permeability and flow.

2. METHODS

2.1 PFLOTRAN

We used the reactive transport code PFLOTRAN to model a simplified 2-dimensional EGS system. PFLOTRAN is a parallelized multiphase reactive transport code that solves well-known governing equations relating to subsurface fluid flow and transport (e.g. multi-phase Darcy's Law with buoyancy, energy, and advection-dispersion including reactive geochemistry) as partial differential equations to treat nonlinear and tightly-coupled flow and geochemical processes in an equivalent continuous porous medium (ECPM) (Hammond et al. 2014; Steefel et al. 2015). PFLOTRAN has previously been used to investigate a number of processes including CO_2 sequestration, geothermal processes, radioactive waste repositories, and other hydrogeological systems (Lichtner and Karra 2013; Hammond et al. 2014; Karra et al. 2014; Steefel et al. 2015; Mariner et al. 2016; Hadgu et al. 2017; Chang et al. 2021). PFLOTRAN's ability to consider flow of variable density fluid through a porous medium together with thermodynamic and kinetic processes such as mineral dissolution/precipitation make it a useful tool to explore the relationship between fluid transport and fracture aperture in a representative subsurface EGS simulation.

In this work, a new PFLOTRAN process model was developed which automatically creates an ECPM representation of a set of discreet fractures, each defined by an initial facture aperture, geometric orientation, and position in space. In each grid cell of the ECPM domain containing one or more fractures, the porosity and permeability is calculated as a function of fracture aperture(s). First, the fracture permeability K^f (m^2) in the orientation of the fracture plane is calculated according to:

$$\mathrm{K}^{\mathrm{f}}_{\mathrm{xx}} = \mathrm{K}^{\mathrm{f}}_{\mathrm{yy}} = \frac{1}{12} f_a^3 \mathrm{h}^{-1} \tag{1}$$

$$\mathrm{K}^{\mathrm{f}}_{\mathrm{zz}} = 0 \tag{2}$$

where f_a (m) is the fracture aperture and h (m) is the grid cell length. In the orientation of the fracture plane, only the *xx* and *yy* components are non-zero. Next, the fracture permeability tensor is rotated into the domain orientation to calculate the anisotropic permeability tensor for the ECPM grid cell. Each rotated fracture permeability is added to the intrinsic matrix rock permeability such that ECPM grid cells containing one or more fractures increase in permeability along the axis of the fracture orientations. Only the diagonal components of the resulting anisotropic permeability tensor are considered for flow calculations. The fracture porosity θ^f (m^3 m^{-3}) for each fracture is calculated according to:

$$\theta^f = f_a / h \tag{3}$$

and added to the intrinsic matrix rock porosity such that ECPM grid cells containing one or more fractures increase in porosity.

Matrix rock thermal expansion and contraction were added to consider changes in fracture aperture with temperature evolution and its effect on the ECPM permeability field[1]. In each ECPM grid cell that contains one or more fractures, the change in matrix length due to thermal expansion or contraction is calculated at the end of each time step as:

$$\Delta L = \alpha \Delta T L \tag{4}$$

where ΔL (m) is the change in material length, α is the material thermal expansion coefficient (m m^{-1} °C^{-1}), ΔT (°C) is the temperature change, and L is the original length of the material perpendicular to the fracture. Next, a new fracture aperture is calculated using ΔL, and the permeability field is updated according to Equation (1), Equation (2) and the procedure immediately following. In the next time step, flow and transport is solved using the updated permeability field. In this design, the fracture process model is sequentially coupled to flow and transport.

In addition to the governing equations pertaining to flow and transport (e.g. as described in Steefel et al. (2015)), this work necessitated consideration of changes to porosity, permeability, and tortuosity given changes in mineral volume fraction, as well as changes in fracture aperture due to matrix thermal contraction. Mineral dissolution and precipitation are calculated given reactive surface area and assigned kinetic rates (Lichtner et al. 2015; Xie et al. 2015; Lichtner 2016). Porosity is updated at each time step as the porosity of the control volume at the prior timestep minus the total change in volume fraction of each mineral (Xie et al. 2015). Permeability is then updated assuming a modified Carman-Kozeny relationship (Xie et al. 2015; Poonoosamy et al. 2021). Updated tortuosity at each new timestep is also calculated as a function of the updated porosity, using Archie's Law (Xie et al. 2015; Poonoosamy et al. 2021).

[1] While changes in porosity also occur with thermal expansion or contraction, in this work porosity did not change as a function of fracture aperture beyond the initial porosity assignment. Including porosity updates will be the topic of future work.

Considerable effort was spent in development to ensure the changes in permeability and porosity due to geochemistry were preserved in addition to the changes in permeability due to thermal effects when both process models were used together[2].

2.2 Model domain, boundary conditions

The base of the domain was set at 4115.25 m below land surface and the top of the domain was set to 3884.75 m below land surface. The initial temperature was set with a gradient of 0.06° C m^{-1} such that temperature increased from 222.5° C to 233.5° C from the top to the bottom of the domain. Initial pressure was set to hydrostatic and increased from 36.0 MPa to 37.9 MPa from the top to the bottom of the domain. Grid cell volumes ranged from 5.0 m^3 near the outer boundaries and were progressively refined to 0.25 m^3 towards the fracture zone for a 2D model domain 150 m in the x-direction, 0.5 m in the y-direction, and 230.5 m in the z-direction. The fracture zone was between the depths of -3999.75 m and -4000.25 m, extended horizontally for 125 m (between x = 20.0 m and x = 130.0 m), and encompassed the entire width of the domain (0.5 m). Injection and production wells with screen length of 0.5 m were set at 24.5 m and 125.5 m along the fracture zone for a production flow path of 100 m. A high permeability production well zone 1.0 m in length and 0.5 m in width extended vertically from the production screen to the surface (fig. 1).

Material properties of granite were assumed for the matrix rock with thermal conductivity of 1.40 W m^{-1} °C^{-1} when dry and 2.75 W m^{-1} °C^{-1} when wet, density of 2.8 g cm^3, and specific heat of 0.9 Jg^{-1} K^{-1} (Heuze 1983; Miao et al. 2014). Porosity and permeability of the (unfractured, intact) matrix rock was set to 0.05 and $1.0 \cdot 10^{-18}$ m^2, and for the well zones was set to 0.7 and $1.8 \cdot 10^{-8}$ m^2 (Selvadurai et al. 2005). Tortuosity was set to 1 for all materials. The initial fracture aperture was set to 3 mm and permeability of the ECPM fracture zone was calculated by PFLOTRAN as $1.32 \cdot 10^{-10}$ m^2 in the horizontal (x and y) and remained $1.0 \cdot 10^{-18}$ m^2 in the vertical (z). The thermal expansion coefficient for granite was set to $40 \cdot 10^{-6}$ m m^{-1} °C^{-1} (Heuze 1983). Fluid was injected at 80° C into the fracture zone at a rate of $3.0 \cdot 10^{-3}$ kg s^{-1}, which is equivalent to a real-world EGS system containing approximately 10 fractures, each 100 m in width, and a production rate of 60 kg s^{-1} (Olasolo et al. 2016; White et al. 2018; Yan et al. 2018). The simulations were run for thirty years.

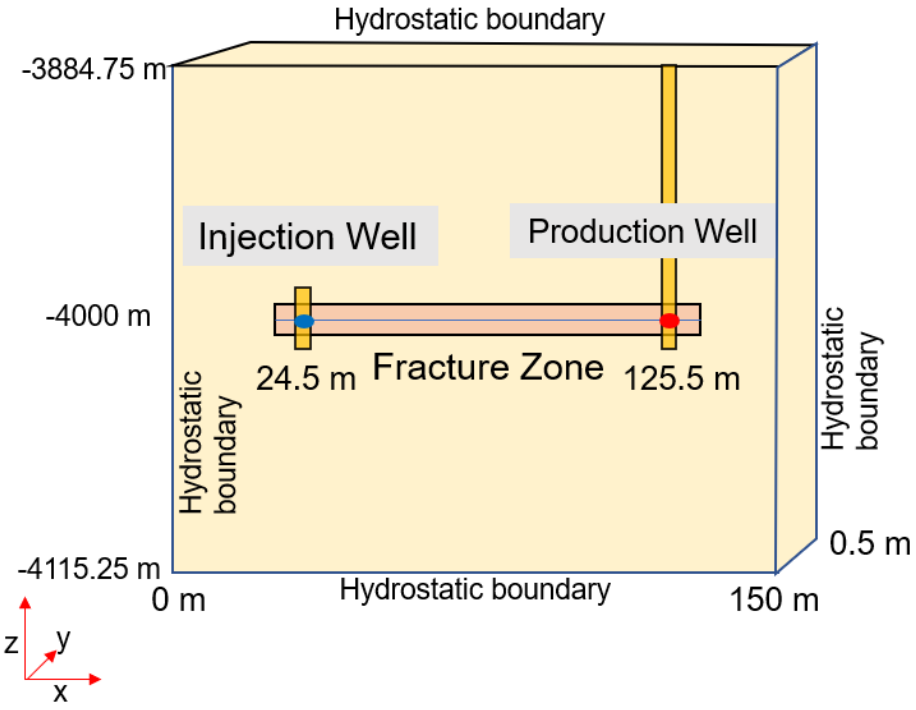

Figure 1: Conceptual model.

2.3 Reaction network

The reaction network was simplified to consider only the calcite system as a minor phase in granite, with the remainder of the "granite" matrix assumed chemically inert. Chemical components included Ca^{2+}, HCO_3^-, $H_2CO_3^{2-}$, H^+, OH^-, $CO_{2\,(aq)}$ and $CO_{2(g)}$. Initial concentrations of Ca^{2+} and other components in both the model domain and the injection fluid were set in equilibrium with a matrix rock assumed to contain 0.04 volume fraction calcite (Worley and Tester 1995; White et al. 2005), for an initial Ca^{2+} concentration of $5.8 \cdot 10^{-4}$ mol L^{-1}. Initial pH was set to 7.1. These initial concentrations are within range of those reported in groundwater wells near the Utah FORGE site (Moore 2016; Blankenship and Ayling 2018).

[2] In other words, changes made by the reactive transport process model did not overwrite changes made by the fracture process model, and vice versa.

The reaction rate for mineral dissolution and precipitation is calculated based on transition state theory, where the overall reaction rate I_m is a function of parallel reaction paths, the mineral's kinetic rate constant, pH, the mineral's equilibrium constant, specific mineral surface area, and the reaction quotient, Q_m (See Lichtner et al. 2015; Lichtner 2016 for further detail regarding these equations). For this work, a temperature and pressure dependent rate constant k_m was calculated from the Arrhenius Equation, with log k calcite at 25° C as -5.81 and activation energy as 23.5 kj mol^{-1} under neutral pH and log k calcite as -0.30 and activation energy as 14.2 kg mol^{-1} under acidic pH (Palandri and Kharaka 2004; Lichtner 2016).

2.4 Simulations

Four simulations were run to examine the effect of both matrix thermal contraction and mineral dissolution/precipitation on fracture zone permeability. A thermal-hydrological (TH) simulation acted as a control and included no thermal contraction of the matrix and no geochemistry; the "thermal contraction" (THM) simulation considered mechanical thermal contraction and no geochemistry; the "chemistry" (THC) simulation considered only geochemistry (mineral dissolution and precipitation) and no thermal contraction; and the "thermal contraction and chemistry" (THCM) simulation considered both mechanical contraction and geochemistry. All simulations were otherwise assigned the same boundary and initial conditions.

3. RESULTS

Compared to the base case TH simulation, effective permeability of the fracture zone between injection and production wells for the THM simulation increased up to two orders of magnitude within thirty years, from $1.32 \cdot 10^{-10}$ m^2 to $1.15 \cdot 10^{-8}$ m^2 with the greatest permeability increase near the injection well (fig. 2). Permeability in the fracture zone of the THC simulation decreased half an order of magnitude from the TH permeability to a minimum permeability of $6.6 \cdot 10^{-11}$ m^2, with the lowest permeability closest to the injection well. Fracture permeability for the final simulation (THCM), inclusive of both thermal contraction and mineral dissolution/precipitation, was a maximum of $6.9 \cdot 10^{-9}$ m^2 close to the injection well, and $2.4 \cdot 10^{-10}$ m^2 near the production well. For this combined simulation, fracture zone permeability was an order of magnitude greater than the base case, but half an order of magnitude lower than the simulation without chemistry. The addition of chemistry from the TH to the THC simulation reduced the maximum permeability by 50%, while the addition of chemistry from the THM to the THCM simulation reduced the maximum permeability by 40%.

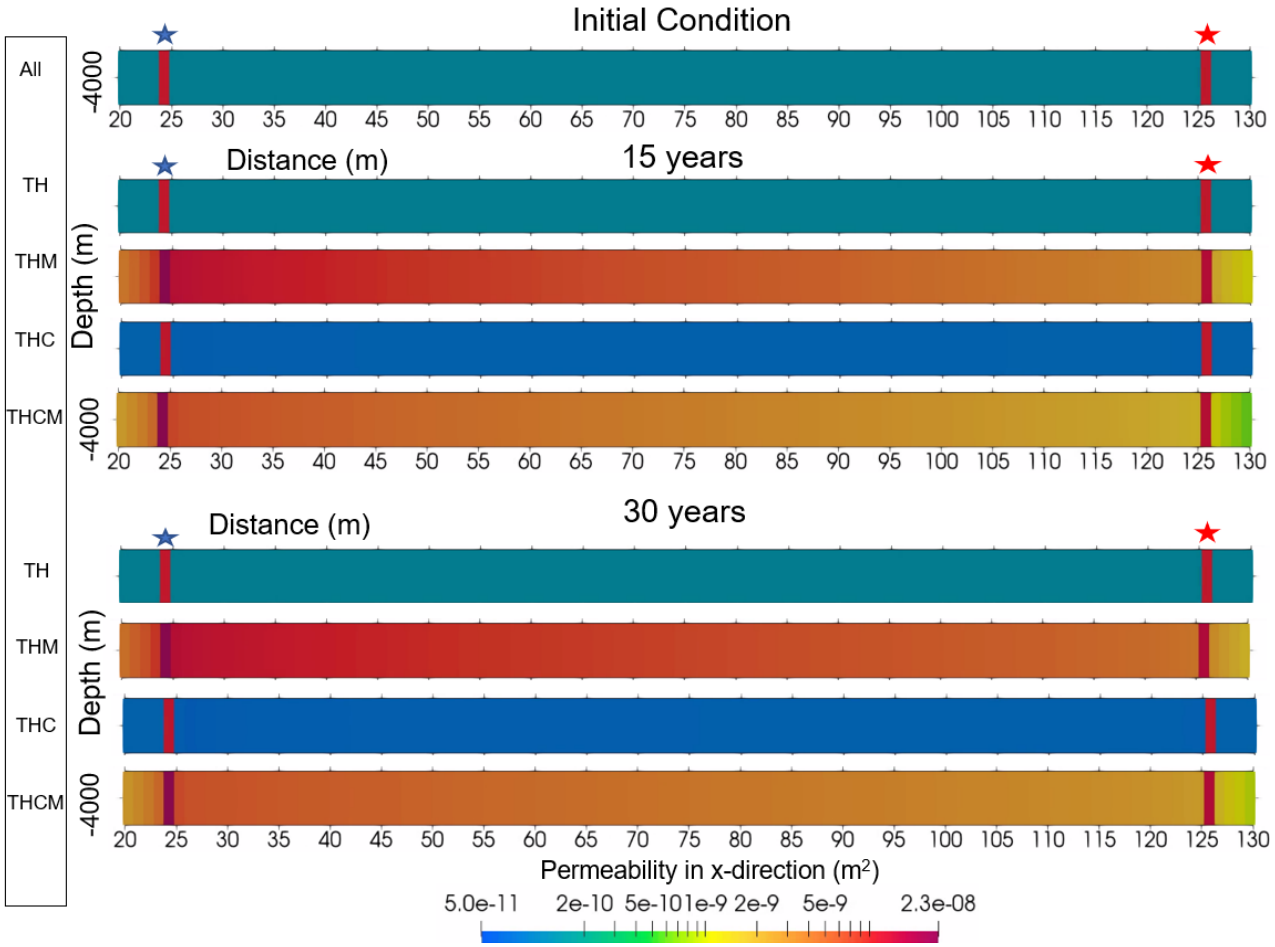

Figure 2: Fracture zone ECPM permeability in the x direction (m^2) for all simulations. Blue and red stars indicate the injection and production wells respectively.

Calcite precipitation was greatest near the injection well in the direction of flow, with volume fraction calcite increasing from 0.040 to 0.047 in both the chemistry simulation and the combined chemistry and thermal contraction simulation. Dissolution also occurred in both simulations with chemistry directly adjacent to the injection well decreasing calcite to below 0.01 volume fraction by the end of thirty years (fig. 3). An additional simulation with injection water at 225° C showed negligible calcite precipitation or dissolution.

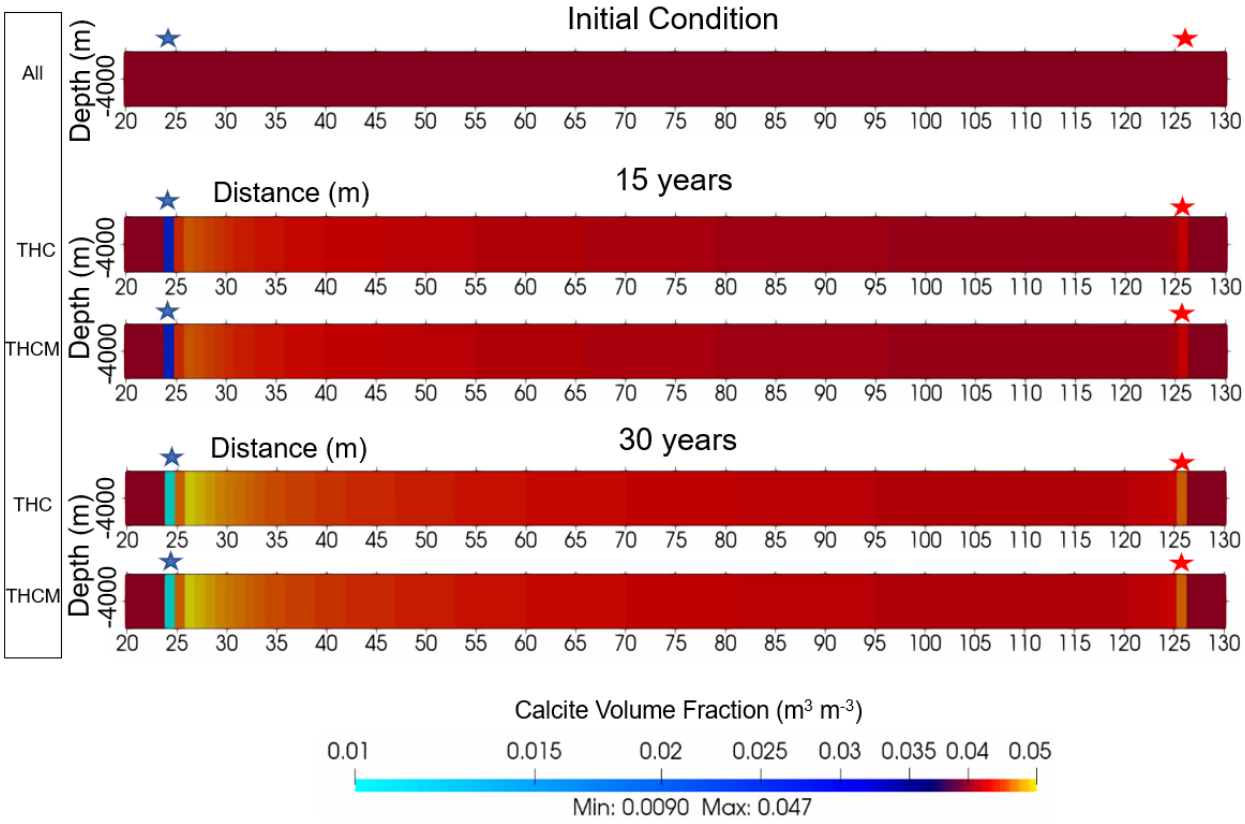

Figure 3: Volume fraction calcite between the chemistry only (THC) and the chemistry + thermal contraction (THCM) simulations. Initial volume fraction calcite was 0.04 and increased to a maximum of 0.047.

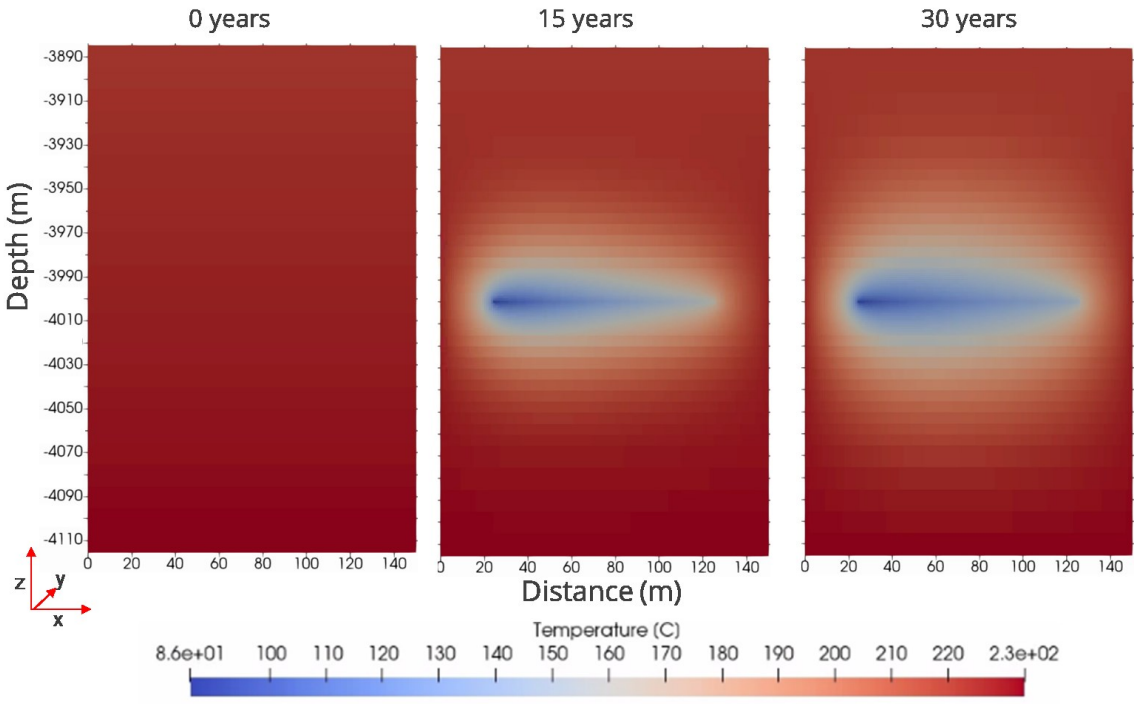

Figure 4: Temperature (°C) between 0 and 30 years for all simulations. Fluid flow is from injection well (left) to production well (right).

Temperature at the production well in the base case TH simulation, which included no change to permeability from either mechanical or chemical processes, decreased from 200° C to 150° C over the course of thirty years (fig. 4, fig. 5). Liquid pressure for the base case TH simulation after thirty years was $3.70097 \cdot 10^7$ Pa at the injection well and $3.70070 \cdot 10^7$ Pa at the production well, for a pressure differential of $3.10 \cdot 10^3$ Pa (fig. 5). Thermal drawdown for the remaining three simulations (THM, THC, THCM) was similar to the base case, but the pressure differential between injection and production wells, was notably different (fig. 6). The liquid pressure at the production well for all simulations at the end of thirty years was the same ($3.7007 \cdot 10^7$ Pa) for all simulations. Liquid pressure at the injection well for the THC simulation was greater than the base case ($3.70119 \cdot 10^7$ Pa), while liquid pressure at the injection well for the two simulations with thermal contraction (TCM and THCM) was lower than the base case ($3.70071 \cdot 10^7$ Pa) (fig. 6).

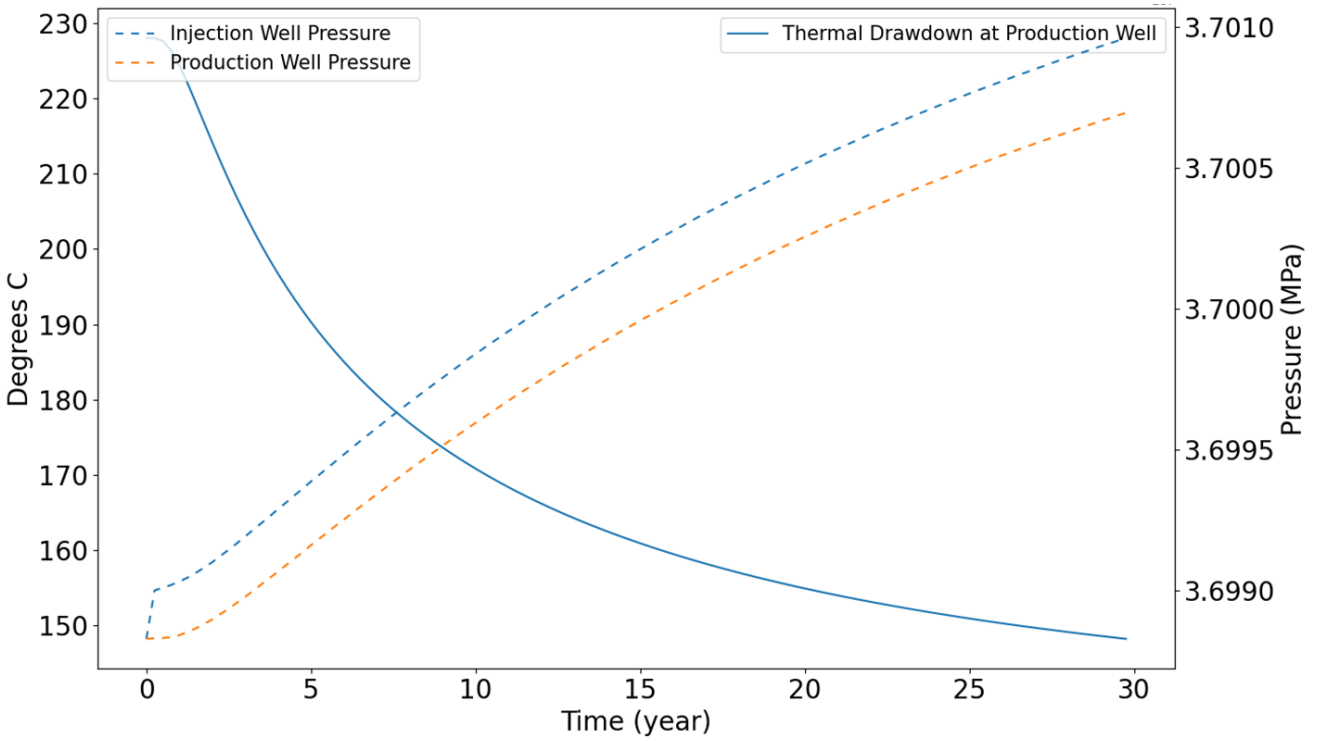

Figure 5: Thermal drawdown and pressure at the injection and production wells for the TH simulation.

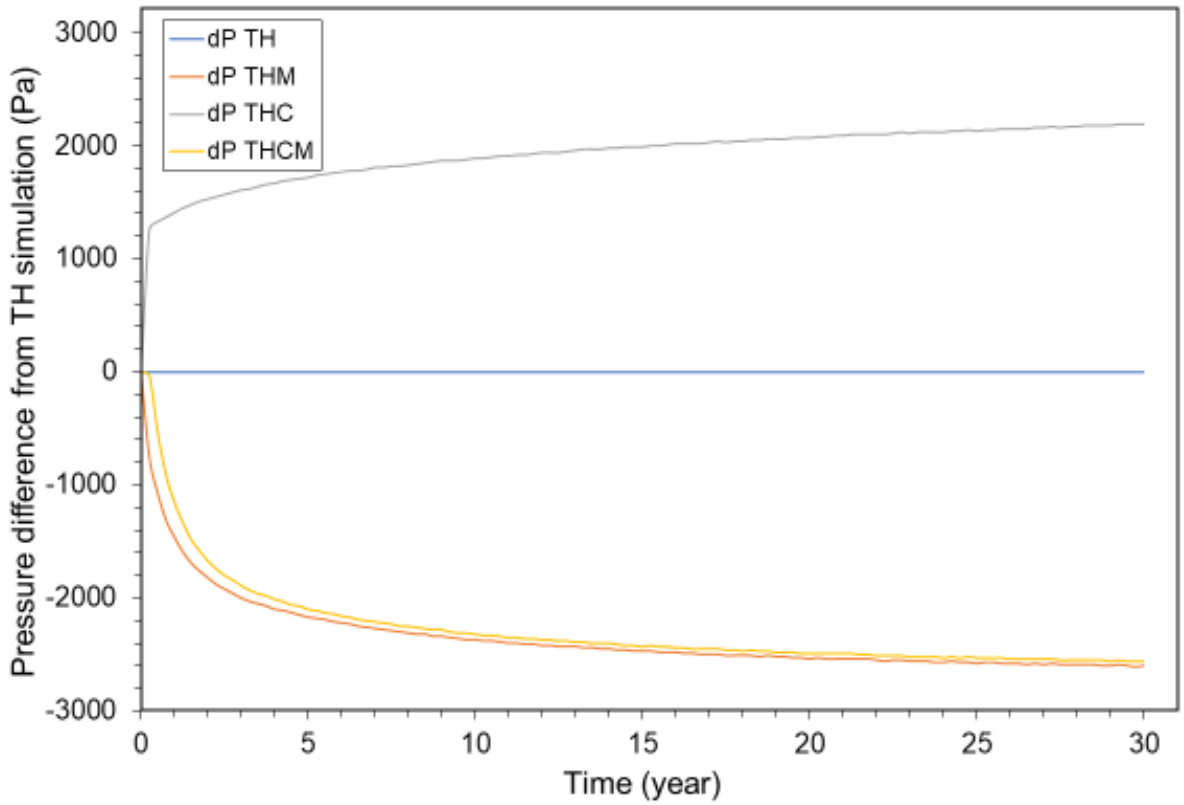

Figure 6: Pressure difference at the injection well between the TH simulation (blue) and the other three simulations (THM, THC, THCM) over 30 years.

4. DISCUSION

This preliminary work suggests that as cool water flows from the injection well to the production well, both mineral precipitation and matrix contraction can have a noticeable effect on fracture zone permeability, with subsequent effects on other aspects of the system, such as pressure. While mineral precipitation decreased permeability in the fracture zone, matrix rock thermal contraction increased fracture zone permeability. When both were considered, thermal expansion of fracture aperture overrode the permeability decrease from precipitation, for a net increase in permeability. This suggests that mechanical changes to the rock matrix may play just as important of a role in controlling flow and transport through a fracture zone as mineral dissolution/precipitation and should be considered as much as geochemistry when modeling fracture flow and EGS. The work here also suggests that matrix rock thermal contraction will "override" the effects of mineral precipitation. However, it should be recognized that the geochemical system represented here is simplified and limited to the calcite system; calcium contribution from other minerals, such as anorthite present in granite, has not been considered, nor has any contribution from silica. A more complex reaction network in future work may show that considering additional reactive minerals will increase the effect of precipitation on permeability and show a greater net permeability decrease even when thermal contraction is included.

Where chemistry and thermal contraction are modeled together versus the simulation with only matrix contraction, the difference in permeability is not simply equal to the permeability change due to mineral precipitation from the simulation with only chemistry. This suggests that there is some feedback between the physical contraction of the rock matrix, expansion of the fracture aperture, and mineral dissolution/precipitation. These feedbacks may be related to processes such as changes in flow velocity as fracture aperture increases, affecting transport rates and thus the rate of precipitation vs dissolution and where mineral precipitation and dissolution may take place (e.g. (Li et al. 2008)), as well as the pressure differences affecting proportion of CO_2 in the aqueous phase. Further investigation into the mechanisms and feedbacks between these two processes will be part of future work.

Injection and production rates are maintained constant for all simulations. When permeability in the fracture zone decreases, there is a subsequent increase in the pressure at the injection wells, suggesting that these permeability decreases due to secondary mineral precipitation can have a negative effect on the amount of work required to maintain a constant pumping rate. Conversely, expanding the fracture aperture through matrix thermal contraction due to cooling may relieve some of this difficulty and make pumping easier. Both processes can impact the economics of an EGS project.

Rough estimates of the LCOE were conducted using an equivalently parameterized hypothetical EGS field that consists of 4 injectors and 8 producers in a 400 m wide reservoir, a 400 m separation distance between injectors and producers, and 10 parallel fractures between each injector and producer. Results show that the changes to the LCOE due only to the changes in effective permeability between the 4 scenarios are minimal, as the thermal drawdown is equivalent and the changes in pumping costs are minor compared to other costs. However, it is expected that the impact on the LCOE will be more impactful for 3-D heterogeneous fracture networks and additional geochemistry processes due to preferential channeling that cause larger variations in the permeability field as well as difference in the thermal drawdown. These processes will be explored as part of the future work of this project.

Finally, the simulation here is representative of what would be only a fraction of a fracture system used for EGS. Future work will require not only a more complex reaction network, but also a larger and more complex fracture network to investigate if and how these processes affecting one fracture can influence what is taking place in other fractures throughout the whole network and, ultimately, the effect on thermal drawdown for an entire enhanced geothermal system.

5. CONCLUSION

The work presented here is a preliminary investigation into the combined effect of thermal contraction and mineral dissolution/precipitation on permeability in the fracture zone of an enhanced geothermal system. It was found that both processes can influence permeability and, when considered together in the same simulation, may override one another, with implications for fluid flow and pumping costs. Future work will include both an upscaled fracture system and reaction network to further investigate the feedbacks between these processes and their overall influence on the viability a full scale, enhanced geothermal system.

Acknowledgements

Sandia National Laboratories is a multimission laboratory managed and operated by National Technology & Engineering Solutions of Sandia, LLC, a wholly owned subsidiary of Honeywell International Inc., for the U.S. Department of Energy's National Nuclear Security Administration under contract DE-NA0003525.

This paper describes objective technical results and analysis. Any subjective views or opinions that might be expressed in the paper do not necessarily represent the views of the U.S. Department of Energy or the United States Government.

SAND2024-01143C

REFERENCES

Blankenship D, Ayling B (2018) Fallon FORGE: Fluid Geochemistry

Chang KW, Nole M, Stein ER (2021) Reduced-order modeling of near-field THMC coupled processes for nuclear waste repositories in shale. Computers and Geotechnics 138:104326. https://doi.org/10.1016/j.compgeo.2021.104326

Chen Z, Feng Z, Mi C, Zhang C (2023) Real-time permeability evolution of limestone under high temperature and triaxial stresses. Geomechanics and Geophysics for Geo-Energy and Geo-Resources 9:1–19. https://doi.org/10.1007/s40948-023-00575-7

Deng H, Spycher N (2019) Modeling Reactive Transport Processes in Fractures. Reviews in Mineralogy and Geochemistry 85:49–74. https://doi.org/10.2138/rmg.2019.85.3

Deng L, Li X, Wu Y, et al (2022) Influence of cooling speed on the physical and mechanical properties of granite in geothermal-related engineering. Deep Underground Science and Engineering 1:40–57. https://doi.org/10.1002/dug2.12011

Dobson PF, Kneafsey TJ, Nakagawa S, et al (2021) Fracture Sustainability in Enhanced Geothermal Systems: Experimental and Modeling Constraints. Journal of Energy Resources Technology 143:. https://doi.org/10.1115/1.4049181

Feng G, Xu T, Wang F, Jiang Zhenjiao (2021) Modeling Analyses of Fluid Flow and Reactive Transport Processes for a Supercritical Geothermal System. In: Proceedings World Geothermal Congress 2020+1. Reykjavik, Iceland

Gringarten AC, Witherspoon PA, Ohnishi Y (1975) Theory of heat extraction from fractured hot dry rock. Journal of Geophysical Research (1896-1977) 80:1120–1124. https://doi.org/10.1029/JB080i008p01120

Hadgu T, Karra S, Kalinina E, et al (2017) A comparative study of discrete fracture network and equivalent continuum models for simulating flow and transport in the far field of a hypothetical nuclear waste repository in crystalline host rock. Journal of Hydrology 553:59–70. https://doi.org/10.1016/j.jhydrol.2017.07.046

Hammond GE, Lichtner PC, Mills RT (2014) Evaluating the performance of parallel subsurface simulators: An illustrative example with PFLOTRAN. Water Resources Research 50:208–228. https://doi.org/10.1002/2012WR013483

Heuze FE (1983) High-temperature mechanical, physical and Thermal properties of granitic rocksıfmmode—\else—\fi A review. International Journal of Rock Mechanics and Mining Sciences & Geomechanics Abstracts 20:3–10. https://doi.org/10.1016/0148-9062(83)91609-1

Huang Y, Pang Z, Kosakowski G (2020) Numerical Study of the Permeability Change Induced by Hot Water Injection in Deep Subsurface Thermal Energy Storage. In: Proceedings World Geothermal Congress 2020+1. International Geothermal Association, Reykjavik, Iceland

Karra S, Painter SL, Lichtner PC (2014) Three-phase numerical model for subsurface hydrology in permafrost-affected regions (PFLOTRAN-ICE v1.0). Cryosphere 8:1935–1950. https://doi.org/10.5194/tc-8-1935-2014

Li L, Steefel CI, Yang L (2008) Scale dependence of mineral dissolution rates within single pores and fractures. Geochimica et Cosmochimica Acta 72:360–377. https://doi.org/10.1016/j.gca.2007.10.027

Lichtner P, Karra S (2013) Modeling multiscale-multiphase-multicomponent reactive flows in porous media: Application to CO2 sequestration and enhanced geothermal energy using PFLOTRAN. In: Computational Models for CO2 Geo_sequestration & Compressed Air Energy Storage. CRC Press, pp 81–136

Lichtner, P. Hammond GE, Lu C, et al (2015) PFLOTRAN User Manual: A Massively Parallel Reactive Flow and Transport Model for Describing Surface and Subsurface Processes

Lichtner PC (2016) Kinetic rate laws invariant to scaling the mineral formula unit. American Journal of Science 316:437–469. https://doi.org/10.2475/05.2016.02

Lima MG, Vogler D, Querci L, et al (2019) Thermally driven fracture aperture variation in naturally fractured granites. Geothermal Energy 7:1–28. https://doi.org/10.1186/s40517-019-0140-9

Mariner PE, Stein ER, Frederick JM, et al (2016) Advances in Geologic Disposal System Modeling and Application to Crystalline Rock

Miao SQ, Li HP, Chen G (2014) Temperature dependence of thermal diffusivity, specific heat capacity, and thermal conductivity for several types of rocks. Journal of Thermal Analysis and Calorimetry 115:1057–1063. https://doi.org/10.1007/s10973-013-3427-2

Moore J (2016) Utah FORGE: Groundwater Data

Ogata S, Yasuhara H, Kinoshita N, et al (2018) Modeling of coupled thermal-hydraulic-mechanical-chemical processes for predicting the evolution in permeability and reactive transport behavior within single rock fractures. International Journal of Rock Mechanics and Mining Sciences 107:271–281. https://doi.org/10.1016/j.ijrmms.2018.04.015

Olasolo P, Juarez MC, Morales MP, et al (2016) Enhanced geothermal systems (EGS): A review. Renewable and Sustainable Energy Reviews 56:133–144. https://doi.org/10.1016/j.rser.2015.11.031

Palandri JL, Kharaka YK (2004) A Compilation of Rate Parameters of Water-Mineral Interaction Kinetics For Application To Geochemical Modeling. U. S. Geological Survey, Menlo Park, California

Poonoosamy J, Wanner C, Alt Epping P, et al (2021) Benchmarking of reactive transport codes for 2D simulations with mineral dissolution–precipitation reactions and feedback on transport parameters. Computational Geosciences 25:1337–1358. https://doi.org/10.1007/s10596-018-9793-x

Rawal C, Gassemi A (2008) Reactive Silica Transport in Hot Poroelastic Rock and its Effects on Fracture Aperture. In: Geothermal Resources Council Transactions. Geothermal Resources Council, Reno, Nevada

Salimzadeh S, Paluszny A, Nick HM, Zimmerman RW (2018) A three-dimensional coupled thermo-hydro-mechanical model for deformable fractured geothermal systems. Geothermics 71:212–224. https://doi.org/10.1016/j.geothermics.2017.09.012

Selvadurai APS, Boulon MJ, Nguyen TS (2005) The Permeability of an Intact Granite. pure and applied geophysics 162:373–407. https://doi.org/10.1007/s00024-004-2606-2

Singurindy O, Berkowitz B (2005) The role of fractures on coupled dissolution and precipitation patterns in carbonate rocks. Advances in Water Resources 28:507–521. https://doi.org/10.1016/j.advwatres.2005.01.002

Steefel CI, Appelo CAJ, Arora B, et al (2015) Reactive transport codes for subsurface environmental simulation. Computational Geosciences 19:445–478. https://doi.org/10.1007/s10596-014-9443-x

Steefel CI, Hu M (2022) Reactive Transport Modeling of Mineral Precipitation and Carbon Trapping in Discrete Fracture Networks. Water Resources Research 58:e2022WR032321. https://doi.org/10.1029/2022WR032321

White AF, Schulz MS, Lowenstern JB, et al (2005) The ubiquitous nature of accessory calcite in granitoid rocks: Implications for weathering, solute evolution, and petrogenesis. Geochimica et Cosmochimica Acta 69:1455–1471. https://doi.org/10.1016/j.gca.2004.09.012

White M, Fu P, McClure M, et al (2018) A suite of benchmark and challenge problems for enhanced geothermal systems. Geomechanics and Geophysics for Geo-Energy and Geo-Resources 4:79–117. https://doi.org/10.1007/s40948-017-0076-0

Worley WG, Tester JW (1995) Dissolution Kinetics of Quartz and Granite in Acidic and Basic Salt Solutions W. Gabriel Worley and Jefferson W. Tester

Xie M, Mayer KU, Claret F, et al (2015) Implementation and evaluation of permeability-porosity and tortuosity-porosity relationships linked to mineral dissolution-precipitation. Computational Geosciences 19:655–671. https://doi.org/10.1007/s10596-014-9458-3

Xu T, Sonnenthal E, Spycher N, Pruess K (2003) Using TOUGHREACT to Model Reactive Fluid Flow and Geochemical Transport in Hydrothermal Systems. In: Geothermal Resources Council Transactions. Geothermal Resources Council, Davis, California

Yan X, Liu Y, Wang G, Lu Y (2018) Optimal injection rate of water in the Guide Basin hot dry rock mining project. Energy Exploration & Exploitation 37:721–735. https://doi.org/10.1177/0144598718800729

Yin T, Li Q, Li X (2019) Experimental investigation on mode I fracture characteristics of granite after cyclic heating and cooling treatments. Engineering Fracture Mechanics 222:106740. https://doi.org/10.1016/j.engfracmech.2019.106740